Ocean Engineering 286 (2023) 115503

Contents lists available at ScienceDirect

Ocean Engineering

journal homepage: www.elsevier.com/locate/oceaneng

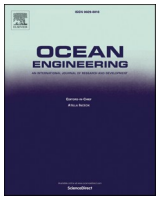

Kinematic motion models based vessel state estimation to support advanced ship predictors

Yufei Wang [a,*], Lokukaluge Prasad Perera [a,b], Bjørn-Morten Batalden [a]

[a] Department of Technology and Safety, UiT The Arctic University of Norway, Tromsø, Norway
[b] SINTEF Digital, Oslo, Norway

ARTICLE INFO

Handling Editor: Prof. A.I. Incecik

Keywords:
Ship maneuvering
System state estimation
Kinematic motion models
Continuous-discrete models
EKF/UKF
Monte-Carlo based simulation

ABSTRACT

Advanced ship predictors can generally be considered as a vital part of the decision-making process of autonomous ships in the future, where the information on vessel maneuvering behavior can be used as the source of information to estimate current vessel motions and predict future behavior precisely. As a result, the navigation safety of autonomous vessels can be improved. In this paper, vessel maneuvering behavior consists of continuous-time system states of two kinematic motion models—the Curvilinear Motion Model (CMM) and Constant Turn Rate & Acceleration (CTRA) Model. Two state estimation algorithms—the Extended Kalman Filter (EKF) and Unscented Kalman Filter (UKF) are implemented on these two models with certain modifications so that they can be compatible with discrete-time measurements. Four scenarios, created by combining different models and algorithms, are implemented using simulated ship maneuvering data from a bridge simulator. These scenarios are then verified through the proposed stability and consistency tests. The simulation results show that the EKF tends to be unstable combined with the CMM. The estimates from the other three scenarios can generally be considered more stable and consistent, unless sudden actions or variations in vessel heading occurred during the simulation. The CTRA is also proven to be more robust compared to the CMM. As a result, a suitable combination of mathematical models and estimation filters can be considered to support advanced ship predictors in future ship navigation.

1. Introduction

In recent years, various interdisciplinary research studies involving modern technologies (machine learning, artificial intelligence, Internet of Things, big data, etc.) have been developed to support the maritime industry and promote its development of autonomous shipping (Akbar et al., 2020; Im et al., 2018; Perera, 2019; Thombre et al., 2022). Several commercial companies and research organizations around the world have already been started relevant research and development activities on the same topic (Kongsberg, 2020; Meguri2040, 2020; Yara, 2021). The establishment of related maritime rules and regulations to deal with autonomous ships is also steadily progressing at the present stage under various maritime authorities to support the same objective (MSC, 2021; UNCTAD, 2021).

The advantages of autonomous ships are believed to be multi-dimensional, while that can also consist of various challenges. Unmanned ship operations indicate that human accommodation and life support facilities can be removed from such vessels, thus more innovative ship structures can be constructed (Kretschmann et al., 2017). The improvements of ship structures can also suggest an increase in energy efficiency and reduce greenhouse gas emissions (Munim, 2019). The shortage of experienced seafarers in shipping can also be mitigated by autonomous ships. (Wróbel et al., 2017). However, challenges posed by autonomous ships will be also there and that can change the status quo of the maritime industry probably to a large extent. The most immediate challenges in autonomous ships can be considered as the safety-related issues in vessel navigation.

The publications from European Maritime Safety Agency show that maritime accidents (collision, contact, and grounding) represent 51.4% of cargo ships from 2014 to 2020 in all sea accidents (EMSA, 2021). To avoid such accidents, accurate and trustworthy collision risk assessment approaches are essential. However, the decision-making process of ship collision avoidance for various vessel encounter situations can be complicated in a mixed environment, where autonomous, manned, and remote-controlled ships coexist, resulting higher collision risk navigation situations (Perera and Murray, 2019). It should be also pointed out that compared with manned ships, where the COLREGs can be used to

* Corresponding author.
E-mail address: yufei.wang@uit.no (Y. Wang).

https://doi.org/10.1016/j.oceaneng.2023.115503
Received 6 March 2023; Received in revised form 1 July 2023; Accepted 29 July 2023
Available online 14 August 2023

Nomenclature

Variables

a_t, a_n	the tangential and normal acceleration components with respect to the course-speed vector
a_u, a_v	the transitional surge and sway acceleration components
$\boldsymbol{K}$	the Kalman gain
$\boldsymbol{N}$	the total iterations of a Monte Carlo-based simulation
$\boldsymbol{P}$	the states covariance
p_x, p_y	the northing and easting positions of the ship's CG in the UTM
$\boldsymbol{Q}$	the covariance matrix of system noise
$\boldsymbol{R}$	the covariance matrix of measurement noise
r	the yaw rate of ship
$\boldsymbol{S}$	the innovation covariance
(t)	the continuous-time unit
$[t_k]$	the discrete-time unit
u, v	the surge and sway velocity components
$\boldsymbol{V}$	the course-speed vector of the ship
v_x, v_y	the velocity components in northing and easting
$\boldsymbol{w_x}$	the white Gaussian system noise
$\boldsymbol{w_z}$	the white Gaussian measurement noise
z_{au}, z_{av}	the measured surge and sway acceleration from the onboard IMU
z_{px}, z_{py}	the measured positions
z_r	the measured yaw rate
z_ψ	the measured heading
α	the significance level of hypothesis test
Δt	the sensors sampling period
δt	the time step for temporal discretization
ε_z	the normalized innovation squared
λ	the initial parameter in the UKF
ψ	the measured heading
ρ	the autocorrelation function
χ	the course of a ship

Subscripts

$\blacksquare_i$	the i-th state in a state vector
$\blacksquare_{ii}$	the i-th diagonal element in a diagonal matrix
$\blacksquare\|_{\{B\}}$	variables described in the vessel body-fixed frame
$\blacksquare\|_j$	the j-th iteration in Monte Carlo-based simulations
$\blacksquare\|_{t_{k-1}\|t_k}$	prior estimates of variables in prediction steps
$\blacksquare\|_{t_k\|t_k}$	posterior estimates of variables in filtering steps

Superscripts

$\hat{\blacksquare}$	the variable with estimated value

Acronyms

CG	Center of Gravity
CMM	Curvilinear Motion Model
CTRA	Constant Turn Rate & Acceleration (Model)
DoF	Degree of Freedom
EKF	Extended Kalman Filter
IMU	Inertial Measurement Unit
NIS	Normalized Innovation Squared
RMS	Root Mean Squared
UKF	Unscented Kalman Filter
UTM	Universal Transverse Mercator

make the respective collision avoidance decisions, there are still no relevant legal frameworks specially designed for autonomous ships (Kim et al., 2022). On the other hand, required ship technologies to support autonomous ship navigation should also be developed, in parallel to the maritime rules and regulations. Therefore, advanced ship predictor type technologies should be considered to support decision support systems for all kinds of vessels under complex navigation situations (Perera, 2019).

1.1. Ship motion prediction

The prediction methods in ship motions can be different and can also influence the respective prediction time horizon. These time horizons can be classified under both local and global prediction scales. For vessel trajectory predictions in a global scale (e.g., a period more than three or more minutes), the AIS data of vessel maneuvering can be utilized to make the required trajectory predictions (Perera and Murray, 2019). This can also be supported by accurately estimating vessel behaviors within a shorter time horizon, which can be viewed as trajectory predictions on a local scale. The improvements in situation awareness (SA) are also vital in the decision-making processes of ship navigation and collision avoidance, and that can also be supported by the same prediction methods. According to the definition of SA, the perception of information from the respective measured data sets is defined as the level one of SA (Endsley, 1995). The failure of SA at level one is reported as the main reasons for many industrial accidents, such as aviation (Grech et al., 2002), offshore drilling (Sneddon et al., 2006), and collisions between attendant vessels and offshore facilities (Sandhåland et al., 2015). From this aspect, a precise estimation of vessel behaviors should be guaranteed to enhance SA in future vessels, i.e., autonomous ships.

Regarding ship maneuvering behavior predictions, the required mathematical concepts are still to be developed due to complex motions of vessels, and some of such challenges are listed in this section. The first one is nonlinear maneuvering behaviors of ships, such as the underactuated property (Do and Pan, 2009). The induced external forces and moments caused by irregular waves or wind can also bring additional complexity in nonlinear ship maneuvering behaviors (Janssen et al., 2017). The second issue lies in the implementation of simplistic mathematical models, which are mainly employed in ship behavior prediction (Perera, 2017). These models are assumed to operate under constant state and parameter conditions; therefore, their performance may be degraded when exposed to varying environmental conditions. It should be also noted that many ship maneuvering behavior prediction applications from bridge systems are supported by the Automatic Radar Plotting Aid (ARPA) and Electronic Chart Display and Information Systems (ECDIS), where linear estimations of vessel positions through a point representation are executed. Such linear estimations can also be problematic in complex navigation environments since not only vessels' positions but also orientations need to be considered in closed encounter situations. That information can also be used to estimate the navigation risk in ship encounter situations.

1.2. Ship maneuvering models

State estimation typically begins with creating mathematical models of the relevant systems. Traditionally, systems are modeled based on the governing laws of nature, also known as physics-based models, which regulate how the systems change over time. More recently, data-driven models have also been developed as an alternative approach. Advances in artificial intelligence and big data technologies make this method more feasible in some applications. A data-driven model can be created by utilizing real data collected from real-world applications, without relying on an underlying physical law. Several recent studies provide a succinct comparison between these two methods (Rahman et al., 2018; Willard et al., 2020).

Data-driven models have been considered to be an effective method in many maritime-related fields (Coraddu et al., 2019; Murray and Perera, 2020; Triepels et al., 2018). However, a major restriction of this approach is that a large number of high-quality data sets should be available, and such data sets can be difficult to obtain or may have low data quality due to limitations in some real-world sensor and data acquisition systems. Another drawback is that data-driven models may have low interpretability or trustworthiness; the contributing factors that cause errors and faults can be thus difficult to identify in some situations (Chakraborty et al., 2020; Ribeiro et al., 2016; Vellido et al., 2012). One should also note that modern data-driven techniques will continue to emerge, resulting in various analysis results based on big data. There are studies that integrate physics-based and data-driven modeling applications have also been proposed (Hanachi et al., 2019; Wang et al., 2022a), yet the availability of large high quality data sets is still mandatory in such applications.

For physics-based models of ship maneuvering, the Newton's laws of motion can be considered as a fundamental concept. The ship maneuvering models can be classified into kinematic and dynamic motion models. The term "kinematics" here refers to the studies of ship motions regardless of external forces and moments that cause it, whereas "dynamic" indicates the influences of external forces and moments into ship maneuvering models. General mathematical expressions of dynamic motion models for ship maneuvering can be seen in recent studies (Fossen, 2010), where most of these expressions are a set of dynamic system equations. The maneuvering model group (MMG) is another dynamic model approach, where the rudder deflection angle and propeller revolutions are used as the model inputs and proposed by Yasukawa and Yoshimura (2014). For a vessel state estimation process, the implementation of dynamic motion models can introduce additional challenges as discussed before. This is mainly due to nonlinear hydrodynamic forces and moments which can be a part of the dynamic motion models but difficult to be measured directly and accurately by on-board sensors (Perera and Murray, 2019). Without adequate sensor measurements, certain iterative estimation algorithms may not converge and thus fail to capture vessel behaviors. A more common way that determines related hydrodynamics coefficients of external forces and moments is to calculate through model scale tests in towing tanks or ocean basins, and then to extrapolate the respective results into full scale vessels. However, such approach may not be accurate due to system-model related erroneous conditions, also not to mention various navigation and environmental conditions which can alter hydrodynamic coefficients of forces and moments significantly due to their time-varying nature.

By using kinematic motion models, model identification difficulties due to external forces and moments can be avoided. The measurements obtained from vessel translational and rotational motions can be used with the mathematical models, i.e., kinematic motion models, directly in such situations, and the variations in accelerations can be considered as model uncertainties. As for the applications of trajectory prediction and then the utilization of the same for collision detection, the models which describe related motions in curved paths under planar motions (Best and Norton, 1997; Li and Jilkov, 2003) are more general. From the view of vehicle maneuvers, the planar motions models indicate three DoFs (i.e., surge, sway, and yaw) and the respective model states represent the relevant maneuvering behaviors (Schubert et al., 2008; Stellet et al., 2015).

1.3. Vessel state estimation

The Kalman filter (KF) is a widely used estimation algorithm for linear systems, and it has extensions for nonlinear systems, such as the extended Kalman filter (EKF) and unscented Kalman filter (UKF) (Daum, 2005; Wan and Merwe, 2000). To use Kalman filter-based algorithms, it is necessary to represent related systems in a state space form. This involves expressing the evolution of state variables through a collection of first-order differential equations that represent the system models. Measurable states are represented as outputs and used to create measurement models. Because of the digital nature, measurement models are frequently applied with the sensor measurements collected in discrete-time. In contrast, many system models can be represented in continuous-time since many mechanical systems are analog. A combination of system and measurement models but with different time representations is also proposed in the recent research studies (Leander et al., 2014; Mbalawata et al., 2012).

When dealing with nonlinear systems, it can be challenging to obtain analytical solutions for nonlinear differential equations in continuous-time system models. Therefore, the temporal discretization technique is necessary to generate numerical solutions, even though they may contain some degree of truncation errors. The order of the truncation errors is positively correlated to the magnitude of the time step (δt) used in the temporal discretization (Ames, 1977). The most common case is to use the δt which is equal to the sampling period of the respective data acquisition system that collects the sensor data (Δt). However, this method is not always reliable because Δt has limitations such that a small value of $\boldsymbol{\delta t}$ may introduce high level of sensor noise. Additionally, using a small value for Δt can introduce unnecessary noise and redundancy, which is not preferable in estimation algorithms either (Miguel et al., 2017). On the other hand, choosing a larger value for δt can lead to unstable numerical solutions, which may cause estimation algorithms to become unstable and diverge (Butcher, 1996).

In some studies, an appropriate value of δt which is usually a factor of Δt is used in the temporal discretization for numerical solutions of nonlinear system models (Frogerais et al., 2012; Sarkka, 2007; Takeno and Katayama, 2012). The EKF and UKF thus need modifications that each prediction step contains nested iterations based on δt. The Runge–Kutta explicit higher order method is further considered to reduce the truncation errors with less iterations (Frogerais et al., 2012; Takeno and Katayama, 2012). The EKF and UKF with the above-mentioned modifications are considered in this study since the proposed kinematic motion models for ship maneuvering is also highly nonlinear and difficult to find its analytical solutions.

It should also be noted that ships, particularly those with large tonnage, exhibit specific maneuvering behaviors (Molland, 2008). Ocean-going vessels are prone to drift due to underactuated conditions, which can result in potential near-miss or collision situations during navigation (Perera, 2017). Accurate estimation of ships' states, especially in the sway direction in order to find the ship's pivot point, is necessary (Seo, 2016). Consequently, the established state-space models and algorithms must be capable of providing precise estimates under such circumstance. Estimated states in sway direction with a longer convergence period (Perera, 2017), or a large delay and bias (Wang et al., 2022b), need to be avoided.

In this study, vessel maneuvering behavior is described by the system states of two kinematic motion models, where the Kalman filter-based approaches are applied to estimate the same system states. To verify the applied models and estimation algorithms, a two-step approach has been taken. Firstly, the models and algorithms have been verified in the bridge simulator environment, and the lessons learned from this process have been documented in this study. Secondly, the verification and demonstration on the same models and estimation algorithms will be conducted on actual vessel navigation using the UiT autonomous test vessel in a future study. Considering that the verification under simulated environments can be crucial prior to conducting future sea trials in a real environment, this paper focuses on the first step of this process. The paper is organized under the following sections: Section 2 presents the literature review of different system modeling methods and the Kalman filter-based estimation algorithms; Section 3 gives extensive details of the proposed kinematic motion models; Section 4 introduces the proposed state estimation algorithms; Section 5 presents the evaluation methods (Monte Carlo-based simulation, algorithm stability and consistency tests) to verify the performances of the filters; The

simulation results, discussions, and conclusions are shown in the last parts of this paper.

2. Kinematic motion models

Kinematic motion models are selected to capture ship maneuvering behavior in this study. The position, velocity, acceleration, and heading states are the important parameters that can reflect the characteristics of relevant ship maneuvers and have been selected for model development in this study.

2.1. State vectors

In a state-space model, the states of a system can be expressed in a vector form. In this paper, two different navigation state vectors (1) and (2) are used, as they are related to the CMM and CTRA for ship maneuvering (see Fig. 1).

$$\boldsymbol{x} = \left[p_x, p_y, v_x, v_y, \psi, r, a_t, a_n\right]^T \text{(in the CMM)\#} \tag{1}$$

$$\boldsymbol{x} = \left[p_x, p_y, u, v, \psi, r, a_u, a_v\right]^T \text{ (in the CTRA)\#} \tag{2}$$

In both models, the values of p_x and p_y are based on the Universal Transverse Mercator (UTM) coordinate system. The unit in the Cartesian grid layout of the UTM is in meters. In the CMM, the course-speed vector V decomposes along the inertial reference frame into v_x and v_y, whereas along the vessel body-fixed reference frame into u and v in the CTRA. The acceleration at and an are the normal and tangential components with regard to V.

All the states in Fig. 1 are related to the ship's apparent CG. Due to added mass effects, the apparent CG can shift during maneuvers. However, to simplify the mathematical models, an assumption is made that such a shift can be neglected by considering that the ship maneuvers are conducted in calm water conditions. As explained in the following section, since the IMU collects the simulated data from the apparent CG, this is a favorable reference frame for generating the respective mathematical models.

2.2. System models

The CMM and CTRA mathematical models are based on the curvilinear motion equation (3), which can be written as:

$$\dot{\chi} = a_n / V$$

$$\dot{V} = a_t$$

$$\dot{p}_x = v_x = V\cos(\chi)$$

$$\dot{p}_y = v_y = V\sin(\chi)\# \tag{3}$$

This system model has a very flexible generality in that it can reduce to several special cases such as constant velocity linear motion ($a_n = 0$, $a_t = 0$), constant acceleration linear motion ($a_n = 0$, $a_t \neq 0$), constant turn motion ($a_n \neq 0$, $a_t = 0$), and more complex cases, where both a_n and a_t are non-zero (Li and Jilkov, 2003).

The model derivation starts with a reference frame transformation, where v_x and v_y in the local inertial reference frame are represented by u and v in the vessel body-fixed reference frame:

$$v_x = u\cos(\psi) - v\sin(\psi)\# \tag{4}$$

$$v_y = u\sin(\psi) + v\cos(\psi)\# \tag{5}$$

The acceleration components in the local inertial reference frame (a_x and a_y) can be thus written as:

$$a_x = \dot{v}_x = \left.\frac{du}{dt}\right|_{\{B\}}\cos(\psi) - u\frac{d\psi}{dt}\sin(\psi) - \left.\frac{dv}{dt}\right|_{\{B\}}\sin(\psi) - v\frac{d\psi}{dt}\cos(\psi)$$

$$= a_u\cos(\psi) - u\,r\sin(\psi) - a_v\sin(\psi) - v\,r\cos(\psi)\ \# \tag{6}$$

$$a_y = \dot{v}_y = \left.\frac{du}{dt}\right|_{\{B\}}\sin(\psi) + u\frac{d\psi}{dt}\cos(\psi) + \left.\frac{dv}{dt}\right|_{\{B\}}\cos(\psi) - v\frac{d\psi}{dt}\sin(\psi)$$

$$= a_u\sin(\psi) + u\,r\cos(\psi) + a_v\cos(\psi) - v\,r\sin(\psi)\ \# \tag{7}$$

With the combination of (4)-(7), the expressions of a_u and a_v can be further written as:

$$a_u = \left(a_x + r\,v_y\right)\cos(\psi) + \left(a_y - r\,v_x\right)\sin(\psi)\# \tag{8}$$

$$a_v = \left(a_y - r\,v_x\right)\cos(\psi) - \left(a_x + r\,v_y\right)\sin(\psi)\# \tag{9}$$

It should be noted that au and av are translational accelerations that represent the rate of change of u and v in the vessel body-fixed frame of reference. The measurements of the accelerations in both surge and sway directions also contain a rotational accelerations component, which will be derived in the following subsection. A summary of the CMM and CTRA models is shown in Table 1. The system nonlinearity is modeled as a Gaussian-distributed noise with a zero-mean. The determination of the covariance matrix of the Gaussian—$\boldsymbol{Q}$ can be complex

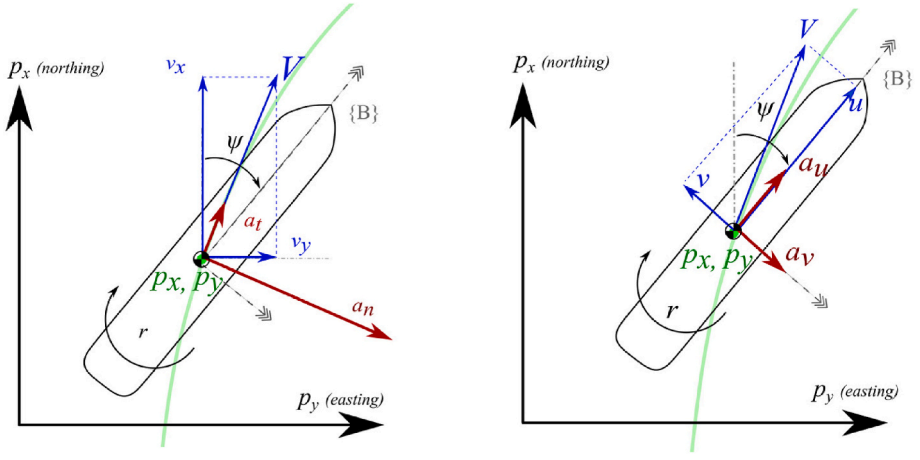

(a) state in the CMM (b) state in the CTRA

Fig. 1. Two different navigation state vectors in the UTM coordinate system. It is assumed that the apparent CG of ship does not shift greatly.

Table 1
System models of ship maneuvering.

Model	CMM	CTRA
state vector	$\boldsymbol{x}(t) = [p_x, p_y, v_x, v_y, \psi, r, a_t, a_n]^T$	$\boldsymbol{x}(t) = [p_x, p_y, u, v, \psi, r, a_u, a_v]^T$
system models with continuous-time step t $\boldsymbol{w}_x \sim \mathcal{N}(\boldsymbol{0}, diag(\boldsymbol{Q}) \in \mathbb{R}^{8\times 8})$	$\dot{\boldsymbol{x}}(t) = f_{CMM}(\boldsymbol{x}(t)) + \boldsymbol{w}_x$ $\begin{bmatrix} v_x \\ v_y \\ a_t f^{vx} - a_n f^{vy} \\ a_t f^{vy} + a_n f^{vx} \\ r \\ 0 \\ 0 \\ 0 \end{bmatrix} + \boldsymbol{w}_x$ $\left(f^{vx} = \frac{v_x}{\sqrt{v_x^2+v_y^2}}, f^{vy} = \frac{v_y}{\sqrt{v_x^2+v_y^2}}\right)$	$\dot{\boldsymbol{x}}(t) = f_{CTRA}(\boldsymbol{x}(t)) + \boldsymbol{w}_x$ $\begin{bmatrix} u\cos(\psi) - v\sin(\psi) \\ v\cos(\psi) + u\sin(\psi) \\ a_u \\ a_v \\ r \\ 0 \\ 0 \\ 0 \end{bmatrix} + \boldsymbol{w}_x$

and sometimes needs experimental data or practical intuition. A general processing method is used with a diagonal matrix to represent $\boldsymbol{Q}$.

2.3. Measurement models

The measurements are from the respective sensors measured by a data acquisition system in discrete-time. Hence, the state variables in the measurement model are discrete. Regarding the measurements, it is considered that the relevant position, heading, yaw rate, and acceleration values of a selected vessel are obtained from the on-board sensors. These sensors can be categorized as GNSS systems, gyroscopes, IMUs, and yaw rate indicators. The multiple measurements can also be written as a vector:

$$z = \left[z_{px}, z_{py}, z_\psi, z_r, z_{au}, z_{av}\right]^T \# \tag{10}$$

The measured positions z_{px} and z_{py} in Eq. (10) are projected from the raw latitude/longitude data into the northing/easting in the UTM coordinate system. One should note that z_{px} and z_{py} indicate the position of the ship's GNSS antenna receivers which may not be the ship's apparent CG. Certain calibration should be done to correct z_{px} and z_{py} to the ship's apparent CG. The elements—z_ψ and z_r are the measured heading (with reference to the axis of northing) and the measured yaw rate (see Fig. 1). These states are available from the fiber optic gyroscope with high precision information. The respective accelerations can be measured by the accelerometers embedded in the IMUs. The mathematical expressions of measured accelerations that are used with respect to a selected vessel with 6 DoFs can be referred in Hover and Michael S (2010). In this study, two assumptions on the IMU are made: its body frame is well aligned with the vessel body-fixed reference frame and it is located close to the vessel's apparent CG. One should note that if these assumption cannot be held in realistic ocean-going vessels, additional mathematical transformations should be introduced to transfer actual measurements into the required model measurements. Furthermore, the acceleration components caused by gravity are also removed from the final outputs of the IMU since heave, pitch, and roll motions are not considered in the motion models. The mathematical expressions of measured accelerations z_{au} and z_{av} can be hence expressed as (11) and (12) when only 3 DoFs are considered.

$$z_{au} = a_u - v\, r \# \tag{11}$$

$$z_{av} = a_v + u\, r \# \tag{12}$$

One should note that the measurement models that have shown in Table 2 share the same measurement vector with a discrete-time step of Δt. The measurement uncertainty is also modeled as the Gaussian noise with a zero mean. Because sensors measure the respective parameters independently, it is reasonable to assume that the covariance matrix of the measurement noise—$\boldsymbol{R}$ is also diagonal. The diagonal elements in $\boldsymbol{R}$ can be determined in advance, e.g., through sensor operation manuals or independent experiments by observing sensor noise conditions.

Table 2
Measurement models.

measurement vector (used by both models)	$z = [z_{px}, z_{py}, z_\psi, z_r, z_{au}, z_{av}]^T$	
Model	CMM	CTRA
measurement models with discrete-time step $t_k = k \bullet \Delta t$ $(k = 1, 2, \ldots)$ $\boldsymbol{w}_z \sim \mathcal{N}(\boldsymbol{0}, diag(\boldsymbol{R}) \in \mathbb{R}^{6\times 6})$	$z[t_k] = h_{CMM}(\boldsymbol{x}[t_k]) + \boldsymbol{w}_z$ $\begin{bmatrix} p_x \\ p_y \\ \psi \\ r \\ h_{u1}\cos(\psi) + h_{u2}\sin(\psi) - v\, r \\ h_{v1}\cos(\psi) - h_{v2}\sin(\psi) + u\, r \end{bmatrix} + \boldsymbol{w}_z$ $(h_{u1} = a_t f^{vx} - a_n f^{vy} + r v_y)$ $(h_{v1} = a_t f^{vy} + a_n f^{vx} - r v_x)$ $(h_{u2} = a_t f^{vy} + a_n f^{vx} - r v_x)$ $(h_{v2} = a_t f^{vx} - a_n f^{vy} + r v_y)$ Where f^{vx} & f^{vy} are shown in Table 1	$z[t_k] = h_{CTRA}(\boldsymbol{x}[t_k]) + \boldsymbol{w}_z$ $\begin{bmatrix} p_x \\ p_y \\ \psi \\ r \\ a_u - v\, r \\ a_v + u\, r \end{bmatrix} + \boldsymbol{w}_z$

3. Estimation algorithms

The EKF and UKF are applied for state estimation under the respective system and measurement models. The parameter estimation process of these two algorithms is usually conceptualized in two steps which execute iteratively: prediction and filtering step. The parameter initialization phase should be included before the parameter estimation process. Since the system and measurement models are described in different time steps, the EKF and UKF algorithms need certain modifications to coordinate the respective iterative steps.

3.1. Time step modification

Since the kinematic-based system models are nonlinear and difficult to obtain analytical solutions, the temporal discretization must be considered. Fig. 2 shows the relationship of various time steps that are considered in this study. In each prediction step, the numerical solutions of prior estimation are calculated through the temporal discretization with δt. The measurements have a sampling period of Δt, so that the measurement innovation, the Kalman gain, and the posterior estimates are calculated every Δt. One should note that the time steps have the units of seconds. An overview of the EKF and UKF with the modifications is illustrated in Figs. 3 and 4. The second-order Runge–Kutta explicit method is used in this study, and further the details can be referred to Frogerais et al. (2012); Takeno and Katayama(2012); Wang et al. (2022b).

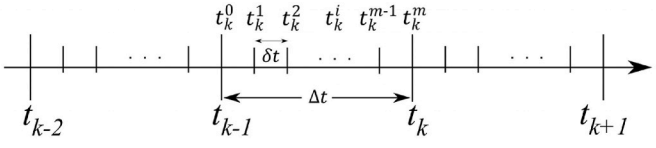

Fig. 2. Time step δt in temporal discretization and measurements sampling period Δt.

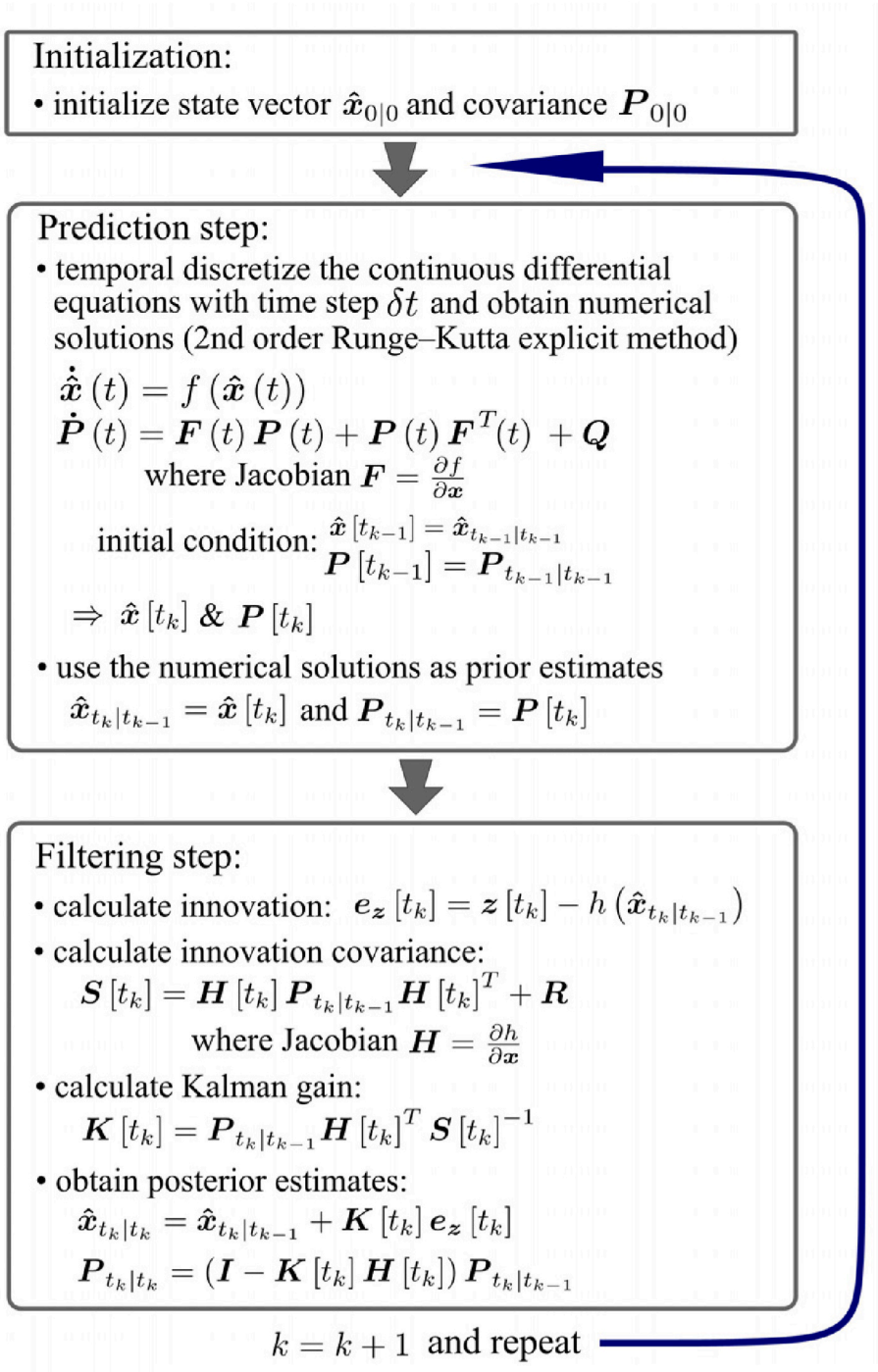

Fig. 3. Chart flow of the EKF.

3.2. State vector initialization

Since the EKF and UKF are suboptimal estimation algorithms, they can diverge in some situations resulted with erroneous estimated parameters (Barrau, 2015). To secure the parameter estimation accuracy, the initial states should be approximately close to the true values as possible. If the initial states are purely guessed and far away from the actual values, the estimation results can diverge. From a practical point of view, some states can be measured directly from sensors. Therefore, the measurements of those states can be used to approximate the initial values of both measurable and non-measurable states. Additionally, it will be explained later that a Monte Carlo-based simulation approach will be used, which allows for multiple iterations with different initialized values within a given parameter range to evaluate the algorithm's performance.

In this study, the initial state vector in each Monte Carlo-based run is randomly generated from a Gaussian distribution (13). This is feasible for initializing the position, heading, and yaw rate values (14)–(15). The velocities in the CMM can be estimated roughly through two historical position values in the beginning (16)–(17). These initialized values can further be used to approximate the respective velocities in the CTRA (18)–(19). All accelerations are initialized as with zero values, since vessel speeds vary relatively slow in general. Therefore, the respective acceleration values should have relatively smaller values.

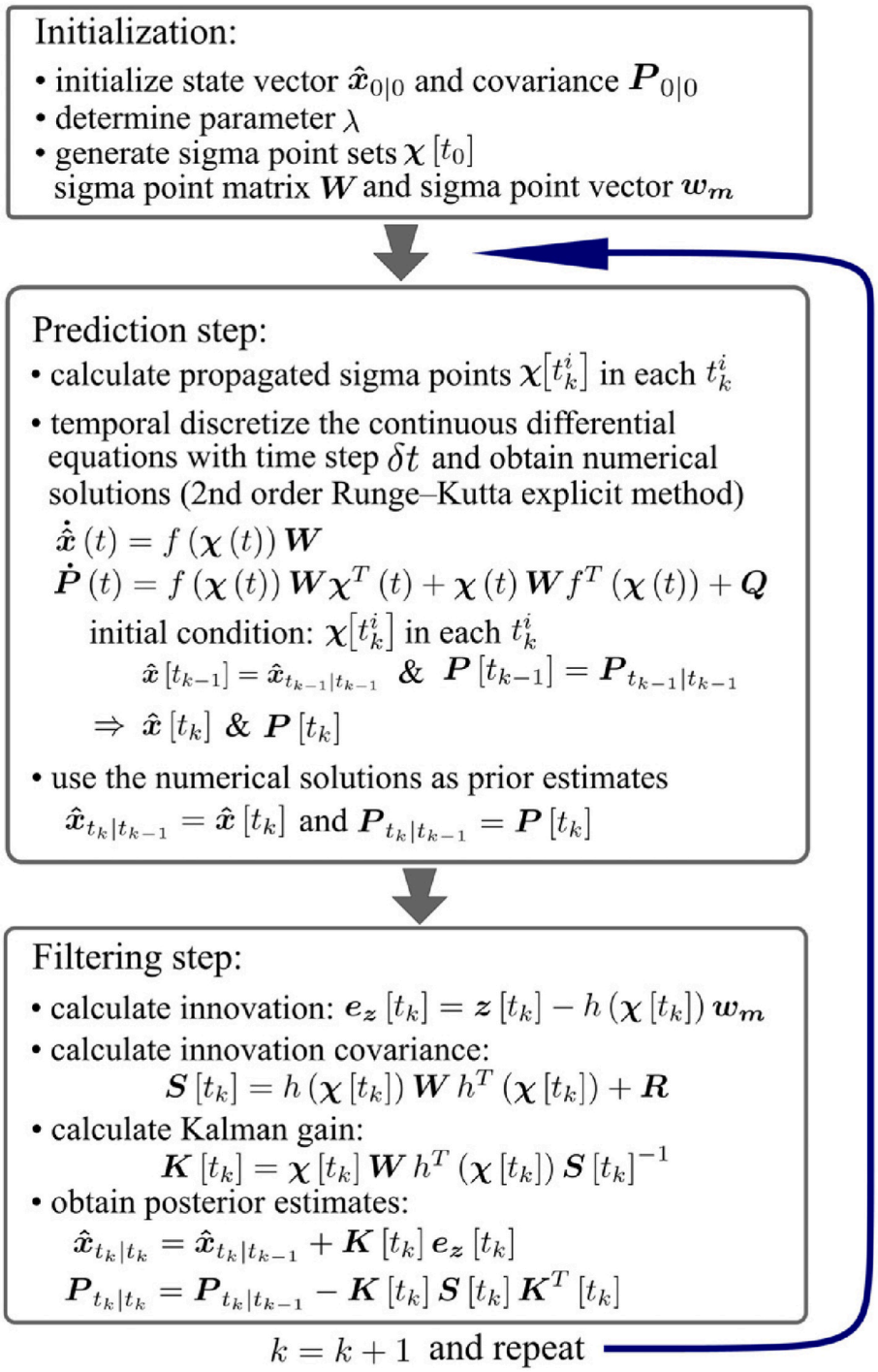

Fig. 4. Chart flow of the UKF.

For $\boldsymbol{P}_{0|0}$, the covariance matrix elements related to the measured states can share the same values as they are in $\boldsymbol{R}$. A two-point differencing method is applied for the correlation between positions and velocities (Bar-Shalom et al., 2002). It should be noted that the initially estimated $\boldsymbol{P}_{0|0}$ is not strictly correct for $\boldsymbol{x}[t_0]$ in the CTRA. The correlations between vessel position and surge/sway velocities can have complex relationships (Svensson, 2019). However, during a normal cruising stage where the sway velocity is not significant compared to the surge velocity, the format of $\boldsymbol{P}_{0|0}$ can be approximately accepted.

$$\hat{\boldsymbol{x}}_{0|0} \sim \mathcal{N}(\boldsymbol{x}[t_0], \boldsymbol{P}_{0|0})\# \tag{13}$$

$$\boldsymbol{x}[t_0] = [z_{px}, z_{py}, v_x, v_y, z_\psi, z_r, 0, 0]^T (\text{for CMM})\# \tag{14}$$

$$\boldsymbol{x}[t_0] = [z_{px}, z_{py}, u, v, z_\psi, z_r, 0, 0]^T (\text{for CTRA})\# \tag{15}$$

$$v_x[t_0] = \frac{z_{px}[t_0] - z_{px}[t_{-1}]}{\Delta t}\# \tag{16}$$

$$v_y[t_0] = \frac{z_{py}[t_0] - z_{py}[t_{-1}]}{\Delta t}\# \tag{17}$$

$$u[t_0] = v_x[t_0]\cos(z_\psi[t_0]) + v_y[t_0]\sin(z_\psi[t_0])\# \tag{18}$$

$$v[t_0] = -v_x[t_0]\sin(z_\psi[t_0]) + v_y[t_0]\cos(z_\psi[t_0])\# \tag{19}$$

$$\boldsymbol{P}_{0|0} = \begin{bmatrix} \boldsymbol{P1}_{4\times4} & \boldsymbol{0}_{4\times4} \\ \boldsymbol{0}_{4\times4} & \boldsymbol{P2}_{4\times4} \end{bmatrix}\# \tag{20}$$

$$\boldsymbol{P1}_{4\times4} = \begin{bmatrix} R_{11} & 0 & \frac{R_{11}}{\Delta t} & \frac{R_{22}}{\Delta t} \\ 0 & R_{22} & 0 & 0 \\ \frac{R_{11}}{\Delta t} & 0 & \frac{2R_{11}}{\Delta t^2} & 0 \\ \frac{R_{22}}{\Delta t} & 0 & 0 & \frac{2R_{22}}{\Delta t^2} \end{bmatrix}\# \tag{21}$$

$$\boldsymbol{P2}_{4\times4} = \begin{bmatrix} R_{33} & 0 & 0 & 0 \\ 0 & R_{44} & 0 & 0 \\ 0 & 0 & R_{55} & 0 \\ 0 & 0 & 0 & R_{66} \end{bmatrix}\# \tag{22}$$

4. Filter verification

The filter verification is implemented to examine the stability and consistency of the estimation algorithms. The necessary data sets used in this study are obtained from simulated ship maneuvers performed in the UiT bridge simulator (see Fig. 5). Ship maneuvers in the bridge simulator are generated from certain dynamic motion models. These models are developed by the respective bridge manufacturer, and these models are unknown for this study. It is assumed that these ship maneuvers are similar to real navigation situations, where the dynamics properties of real ship motions can be difficult to capture precisely.

4.1. Monte Carlo-based simulation

After several ship maneuvering exercises in the bridge simulator, several data sets are collected. That data set consists of vessel states as well as simulated measurements of the respective vessel states. There are four scenarios which are made by different combinations of the models and algorithms are utilized on the same data sets. These scenarios share the same global parameters. Each scenario is executed N times with different initial values and measurements. Such an approach is thus equivalent to offline multiple running, i.e., Monte Carlo-based simulations. Fig. 6 shows how the Monte Carlo-based simulations are performed with the respective scenarios.

The values of the global parameters that are used for the Monte Carlo-based simulation are listed in Table 3. Since there are 50 independent measurements that can be collected, the Monte Carlo-based simulation is run 50 iterations. The sampling period of measurements is 0.1 s. The time step for the temporal discretization is set to 0.005 s, resulting in 20 internal iterations for the numerical calculations in each prediction step. One should note that as the time step for the temporal discretization increases, the numerical solutions from the explicit methods (such as the Runge-Kutta explicit method in this study) can become unstable (Butcher, 1996). Hence, the value of 0.005 s used in this study to satisfy the required stability requirement. The definition of parameter λ in the UKF should be referred to Wan and Merwe (2000).

Fig. 5. UiT bridge simulator.

4.2. Estimation algorithm stability

The Kalman gain $\boldsymbol{K}$ is vital for precise estimation of the vessel states. Since the calculations of $\boldsymbol{K}$ contain the inverse matrix operation of innovation covariance $\boldsymbol{S}$, this matrix should be well-conditioned such that the inverse operation should not be sensitive to the respective perturbations. In this study, the reciprocal condition number (Rcond) is used as a criterion to examine the condition of $\boldsymbol{S}$ (Cline et al., 1979). It can be defined as:

$$Rcond(\boldsymbol{S}) = \frac{1}{\|\boldsymbol{S}^{-1}\|_1 \bullet \|\boldsymbol{S}\|_1}\# \tag{23}$$

$$\text{where, } \|\boldsymbol{S}\|_1 = \max_{1\le j\le \dim(\boldsymbol{S})} \sum_{i=1}^{\dim(\boldsymbol{S})} |a_{ij}|\# \tag{24}$$

If $\boldsymbol{S}$ is well-conditioned, $Rcond\ (\boldsymbol{S})$ is near 1, otherwise an ill-conditioned $\boldsymbol{S}$ will have the Rcond close to 0. One should note that the threshold that determines whether a matrix is well-conditioned depends on the specific problem and the desired level of the parameter estimation accuracy. In this study, the threshold value is set to 1×10^{-10} which is an iteratively observed value. With this threshold value, the small estimated errors can have a major impact on the inverse of $\boldsymbol{S}$. The executions of both algorithms are designed to be interrupted if an ill-conditioned $\boldsymbol{S}$ is detected, where the parameter estimation process can be classified as divergence. If an interruption occurs during the execution of an estimation algorithm, the related algorithm can be thus considered as diverged. It is important to note that an algorithm may not exhibit divergence in a single trial, which is why multiple runs are necessary. This is also why the Monte Carlo-based simulation are implemented in this study.

4.3. Estimation algorithm consistency

The consistency test for estimation algorithms is necessary to verify whether the estimated states converge to the actual states. The calculated innovations $\boldsymbol{e}_z$ can be used to evaluate the consistency of the estimation algorithms. The consistency test should be performed based on simulated data before applying parameter estimation algorithms to real-world data, as actual states may not always be available in real-world applications. The respective criteria for the consistency of an algorithm can be categorized as:

(1) Innovations should be accepted as the zero mean and own magnitude commensurate with the innovation covariance matrix;
(2) Innovations should be accepted as the white Gaussian noise. The normalized innovation squared (NIS) is used to verify the first criteria in general, and it is defined as:

$$\varepsilon_z[t_k] = \boldsymbol{e}_z^T[t_k]\boldsymbol{S}_{t_k|t_{k-1}}^{-1}\boldsymbol{e}_z[t_k]\# \tag{25}$$

For the Monte Carlo-based simulations which provide the (N-run) average NIS $\bar{\varepsilon}_z$, a chi-square test for hypothesis testing can be implemented (Chew, 1966):

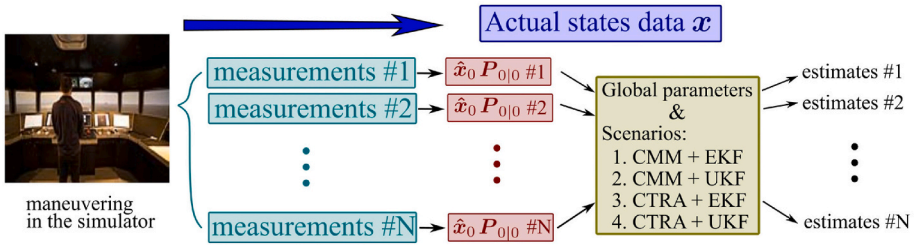

Fig. 6. Monte Carlo-based simulation.

Table 3
Global parameters assignment.

Global parameters	
N	50
Δt	0.1 [s]
δt	0.005 [s]
$\boldsymbol{Q}$	$diag(10^{-1}, 10^{-1}, 10^{-3}, 10^{-3}, 10^{-5}, 10^{-5}, 10^{-1}\pi/180, 10^{-5}\pi/180)$
$\boldsymbol{R}$	$diag(1^2, 1^2, (0.5\pi/180)^2, (10^{-3}\pi/180)^2, 0.01^2, 0.01^2)$
λ	1.72 (only used in the UKF)

H0 criterion (1) is established;
H1 *criterion (1) is NOT established or inconclusive;*

Test statistic:

$\chi^2 = \bar{\varepsilon}_z$ with the DoFs $N \cdot \dim(z)$

Critical value:
(two-sided test with a significant level $\boldsymbol{\alpha} = 0.05$)

$$\left[\chi^2_{N\bullet\dim(z)}(0.025), \chi^2_{N\bullet\dim(z)}(0.975)\right]$$

The (N-run) average autocorrelation $\bar{\rho}$ can be used as the test statistics for the criterion (2), and the Z-test as a hypothesis test can be applied (Bar-Shalom et al., 2002):

H0 criterion (2) is established;
H1 *criterion (2) is NOT established or inconclusive; Test statistic:*

$$Z = \bar{\rho}(k, k+1) = \frac{1}{\sqrt{\dim(z)}} \frac{num_1}{den_1 \ den_2} \# \tag{26}$$

where : $num_1 = \sum_{j=1}^{N} \boldsymbol{e}_z^T[t_k]\boldsymbol{e}_z[t_{k+1}]\big|_j$

$$den_1 = \sqrt{\sum_{j=1}^{N} \left(\boldsymbol{e}_z^T[t_k]\boldsymbol{e}_z[t_k]\right)\big|_j}$$

$$den_2 = \sqrt{\sum_{j=1}^{N} \left(\boldsymbol{e}_z^T[t_{k+1}]\boldsymbol{e}_z[t_{k+1}]\right)\big|_j}$$

Critical value:
(two-sided test with a significant level $\boldsymbol{\alpha} = 0.05$)

$$\left[-1.96 \Big/ \sqrt{N}, 1.96 \Big/ \sqrt{N}\right]$$

One should also note that the EKF and UKF are suboptimal estimation filters. The estimated states may not be optimal in the sense of minimizing the mean squared errors with respect to the true states, where the estimation algorithm can be diverged in some situations. The non-zero estimated errors may be achieved so that the complete consistency is not possible. Therefore, the estimation algorithm consistency test also needs to examine the behavior of the estimation errors. The root mean squared (RMS) errors are used in this study, and the RMS error of a single state x_i in step t_k from the Monte Carlo-based simulations with N-run can be defined as:

$$RMS(x_i[t_k]) = \sqrt{\frac{1}{N}\sum_{j=1}^{N} (\hat{x}_i[t_k] - x_i[t_k])\big|_j \#} \tag{27}$$

where: $x_i[t_k]$ is the actual value in step t_k.

5. Simulation results and discussion

A selected vessel used in the bridge simulator is illustrated in Fig. 7. It is a general cargo ship equipped with a single controllable pitch propeller and a single rudder. The position of the apparent CG is located midships, and it is assumed that the apparent CG does not shift largely during ship maneuvers.

5.1. Simulated ship maneuvers

Several ship maneuvers are conducted in the UiT bridge simulator (see Fig. 8). The trajectory made from these maneuvers is similar to the Williamson turn (Ian, 2004). Calm weather conditions are implemented in the bridge simulator, which means that impacts from wind and waves are insignificant. In addition, the speed of the surrounding ocean currents is also set to be 0 so that the SOG is identical to the STW. Based on the maneuvers, six voyage segments can be divided. These segments include:

S1 (wp1 → wp2) steady-state cruising (11.43 knots with the propeller pitch 0.78);
S2 (wp2 → wp3) place the rudder to starboard with a deflection angle of 35°;
S3 (wp3 → wp4) place the rudder to port with 35° when the heading reaches 90°;
S4 (wp4 → wp5) reduce the rudder to 10 degrees of port when the heading reaches 300°;
S5 (wp5 → wp6) place the rudder amidships when the heading reaches 230°;
S6 (wp6 → end) decrease the propeller pitch to 0.33 when the heading reaches 210°.

Since typical ship maneuvers, such as cruising, turning, and slow-up are all included, the analyses are divided by different time intervals to examine each voyage segment.

5.2. Estimation algorithm stability

The estimation algorithms follow the procedure stated in Section 4.1. The simulation results show that Scenario 1 (the CMM with EKF) is the only unstable combination. The diverged instances in Scenario 1 during the Monte Carlo based simulation with 50 runs are labeled in Fig. 9a. The distribution of the diverged instances illustrates that they mostly occur after the vessel executes a new rudder or propeller order. For a diverged instance, the errors of estimated states (v_x, v_y, ψ, and r) are depicted in Fig. 9b. It can be observed that the errors of $\hat{v}_x$ and $\hat{v}_y$ have significant increases in the middle of the execution period. In the last moments before the interruption, the errors of $\hat{v}_x$ and $\hat{v}_y$ demonstrate a

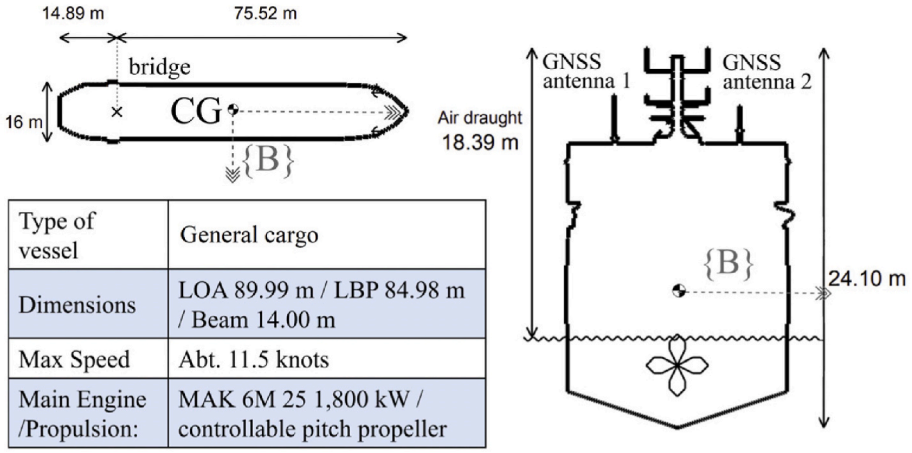

Type of vessel	General cargo
Dimensions	LOA 89.99 m / LBP 84.98 m / Beam 14.00 m
Max Speed	Abt. 11.5 knots
Main Engine /Propulsion:	MAK 6M 25 1,800 kW / controllable pitch propeller

Fig. 7. The vessel used in the simulator.

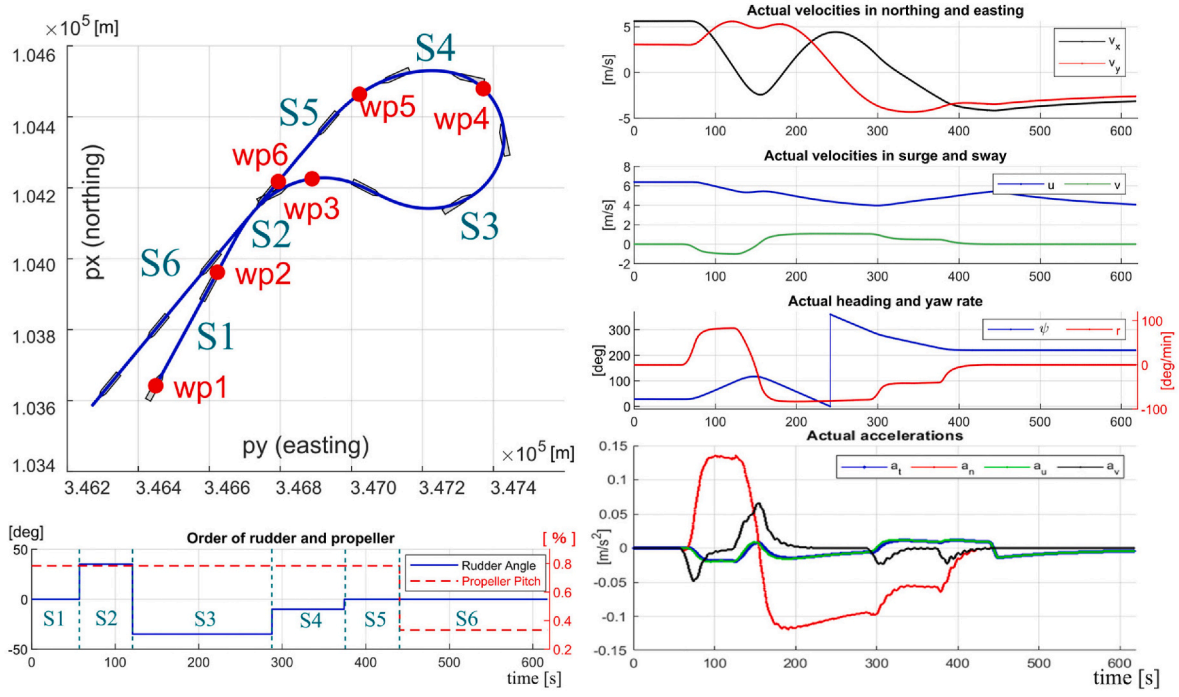

Fig. 8. The simulated maneuver in the UiT bridge simulator. The actual latitude/longitude data sets are transferred into the UTM coordinate system. The vessel icons are shown every 50 s.

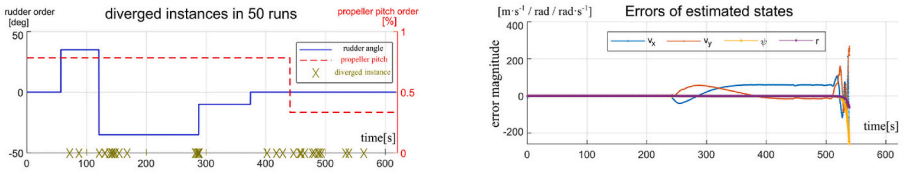

(a).Diverged instances are labeled in the time axis. The labeled positions represent the moments when the interruption occurs.

(b) The error magnitude of estimated states (v_x, v_y, ψ, r) from a diverged instance.

Fig. 9. The stability test results of Scenario 1 (CMM + EKF).

trend of unstable oscillations. Meanwhile, the errors of $\hat{\psi}$ and $\hat{r}$ are showing approximately exponential growth. Since these estimated states contribute to the components of Jacobian $\boldsymbol{F}$ and $\boldsymbol{H}$ in the EKF, $\boldsymbol{F}$ and $\boldsymbol{H}$ can thus diverge and cause the ill condition of $\boldsymbol{S}$ consequently.

The truncation errors from a first order Taylor series expansion in the EKF as well as the nonlinearity in both the system and measurement models of the CMM can be considered as the reasons to introduce such an instability of Scenario 1. Because both estimated prior and posterior error covariances require the $\boldsymbol{F}$ and $\boldsymbol{H}$, the truncation errors thus will remain in the solutions after each iteration. Upon closer examination of

Fig. 9b, it becomes apparent that the estimated errors begin to accumulate to a larger value, which means that the EKF fails to compensate for the estimation errors. The execution of new control orders accelerates the error accumulation processes. In comparison with the UKF in Scenario 2, where the Taylor series expansion is not applied, the respective truncation errors do not impact the solution of the error covariance matrix. Therefore, the unscented transformation in the UKF is clearly more robust for the nonlinearity in the CMM.

It should also be emphasized that the nonlinearity of both the system and measurement models of the CTRA is relatively smooth, compared with the nonlinearities in the CMM. The smoothness can be understood as that the functions in both the system and measurement models of the CTRA are continuously differentiable, and there are no discontinuous or sudden changes of the derivatives. As a result, these functions are well-behaved and mathematically tractable. The EKF can hence converge with the CTRA, as observed in the results. By contrast, the terms f^{vx} and f^{vy} in the CMM indicate that the respective derivatives can exhibit sudden changes as either v_x or v_y approaches 0.

5.3. Estimation algorithm consistency

The (N-run) average NIS and autocorrelation (one step apart) of Scenario 2, 3, and 4 are presented in Fig. 10. As can be seen, there are three unbounded periods that the average NIS is greater than the upper bound in S2 and S3 for all scenarios (over the logarithmic scale). The average NIS only slightly exceeds the upper bound in the first and second periods, whereas a great exceedance can be observed in the last period when the heading switches. For the autocorrelation, there is only one unbounded period which happens in S3.

The percentage of the bounded test statistics are shown in Table 4 and Table 5. Except for S2 and S3, approximately 70%–80% of the average NIS and over 90% of the autocorrelation function are within the critical values. In each voyage segment, it can also be confirmed that there are situations where the average NIS are less than the lower bound (roughly 20%), and these average NIS are evenly distributed and the values do not significantly exceed the lower bound.

When comparing Scenario 2 and 3 (or Scenario 2 and 4), it is perceptible that the average NIS in the first and second unbounded period in Scenario 2 is slightly higher. In the last unbounded period, it takes a longer time for the average NIS converges to the critical value range again in Scenario 2. The autocorrelation shares a similar behavior in that the re-converge time in Scenario 2 is longer. The test results also show that the test statistics of Scenario 3 and 4 are fairly close to each other.

The three unbounded periods overlap within three events: the first and second unbounded periods correspond to the rudder order in S2 and S3; the last unbounded period is due to switching of the vessel heading between 0 to 360°. The first and second events are thought to cause the modeling errors in the CMM and CTRA. Because the mean values of accelerations and yaw rate are assumed to be 0 in both models (see Table 1), and sudden actions (such as rudder to starboard/port with 35°) can produce significant changes of the respective translational and rotational accelerations or yaw rate, there exists thus a discrepancy between the models and the real maneuvering behaviors after these actions. A shorter re-convergence periods can manifest that the CTRA is more robust, whereas the CMM can be sensitive towards sudden actions. The switching of the vessel heading is thought to cause numerical errors in the estimation algorithms. Once the vessel heading is aligned with the true north, the heading measurements of heading can switch between

Table 4
Percentage of the bounded average NIS.

Stages	S1	S2	S3	S4	S5	S6
Scenario 2 (CMM + UKF)	77%	77%	67%	80%	77%	72%
Scenario 3 (CTRA + EKF)	73%	80%	74%	77%	77%	74%
Scenario 4 (CTRA + UKF)	73%	80%	74%	77%	77%	74%

Table 5
Percentage of the bounded autocorrelation.

Stages	S1	S2	S3	S4	S5	S6
Scenario 2 (CMM + UKF)	94%	95%	81%	93%	93%	95%
Scenario 3 (CTRA + EKF)	92%	94%	92%	96%	96%	95%
Scenario 4 (CTRA + UKF)	93%	94%	93%	95%	93%	95%

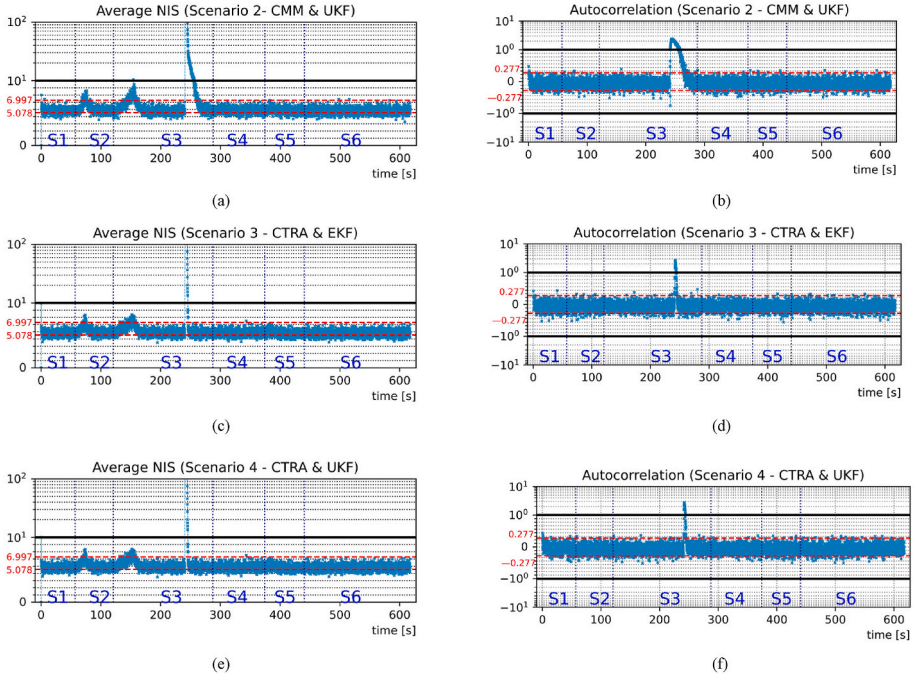

Fig. 10. Filter consistency test based on average NIS and autocorrelation. Areas above and below the black lines are on a logarithmic scale. The related critical values of test statistics are shown in red lines.

0 and 360°, which leads to great numerical errors in the innovation calculations.

Since the upper unbounded values of the NIS indicate that the estimated error can be underestimated, ship maneuvering behavior predictions in a local scale based underestimated errors can be thus too optimistic so that potential collision risks can be overlooked. In contrast, the lower unbounded NIS represents the overestimation of errors, which causes an inefficiency in the estimation algorithm. Since the consistency tests show that the lower unbounded NIS (roughly 20%) is evenly distributed and not significantly exceeded, the impact on the prediction error is considered negligible.

5.4. Root mean square errors

The RMS errors from the Monte Carlo-based simulations of Scenario 2, 3 and 4 are illustrated (see Figs. 11–13). The suboptimal property of proposed nonlinear filters can be used to explain the non-zero RMS errors. One can observe that a modest increase of the RMS errors during the first and second unbounded periods due to the sudden actions. The most significant increases in the RMS errors happen after the switching of the vessel heading. Although both the EKF and UKF can converge the estimation algorithm again, the re-convergence time can be longer for some states, and this is more obvious in Scenario 2. Therefore, it can be inferred that the frequent switching of the vessel heading, such as continuous northward navigation or zigzag maneuvers, can cause large estimation errors and cause estimation algorithms to diverge.

It is also obvious in Figs. 11–13 that the estimation accuracy of velocities and accelerations is guaranteed in the proposed state-space models. The state-space models used in this study validate the speculations that ship motions in the sway direction can have a greater influence on the state estimation process, causing the large drifts and biases in the estimated velocities and accelerations (Wang et al., 2022b). When comparing Scenario 3 and Scenario 4, it can be observed that the performances of the EKF and UKF are almost the same. Since the computational cost of the UKF is usually higher, the EKF can be a better choice for real-time applications with limited computational resources.

Based on the above discussion, it can be considered that Scenarios 2, 3, and 4 are consistent, except for sudden rudder orders or vessel heading variations. To mitigate the estimation algorithm errors due to such sudden actions, an increase in the model uncertainty can be introduced, and such a method requires an adaptive tuning mechanism of the system noise matrix. For vessel heading variations (i.e., between 0 and 360°), a special wrapping treatment towards the vessel heading inside the estimation algorithms should be developed in the future.

6. Conclusion

Two kinematic motion models—the CMM and CTRA are used as the system models in continuous-time for vessel state estimation. Combining with the measurement models in discrete-time, the EKF and UKF with corresponding modifications are applied. Based on the simulated maneuvering data sets from the UiT bridge simulator, the Monte Carlo-based simulations are performed on four scenarios, and the simulation results are further used for the estimation algorithm stability and consistency tests. The results of the stability test show that the combination of the CMM and EKF (Scenario 1) is an unstable scenario. For the other three scenarios, except for periods when sudden maneuvering actions or vessel heading variations occur, the estimation algorithm can be considered as consistent, even though small scale estimation errors exist.

It is apparent that Scenario 1 should be avoided in actual vessel maneuvering situations. For other scenarios, the estimated parameters with a relevant consistent test can be used to evaluate the estimation accuracy of ship maneuvering behavior in a local scale. However, it should be noted that sudden maneuvers of ocean-going vessels can often lead to high-risk ship encounter situations. Due to changes in translational and rotational accelerations or yaw rate caused by sudden maneuvering actions, the vessel state predictions based on the CMM and CTRA may not be sufficient so that potential collision risks may be higher. To increase the prediction accuracy, it may require a large amount of vessel state measurements for a longer period, but this may result in a shorter reaction time for the decision-making process during a ship close encounter situation. Switching of the vessel's heading can cause larger estimation errors compared to sudden maneuvers. It is expected that degraded vessel state predictions may occur after such situations. Therefore, certain methods that can reduce the heading-related errors need to be considered (Wang et al., 2023). Regarding the simulation results, it is worth mentioning that multiple simulations involving different types of vessels are conducted, and they yielded similar results. However, for the sake of representativeness, this paper presents only the results for a general cargo ship.

The bridge simulator-based experiment can be viewed as the foundation for verifying the models and algorithms in the second step. Future work will involve verifying these models and algorithms using real navigation data obtained from sea-trial experiments. It is expected that certain errors may arise during sea trails, especially under rough weather or sea conditions. Furthermore, real vessels equipped with complex control and power systems may exhibit unexpected maneuvering behaviors, which can introduce additional uncertainties. Therefore, further work will be also planned to find solutions for these factors.

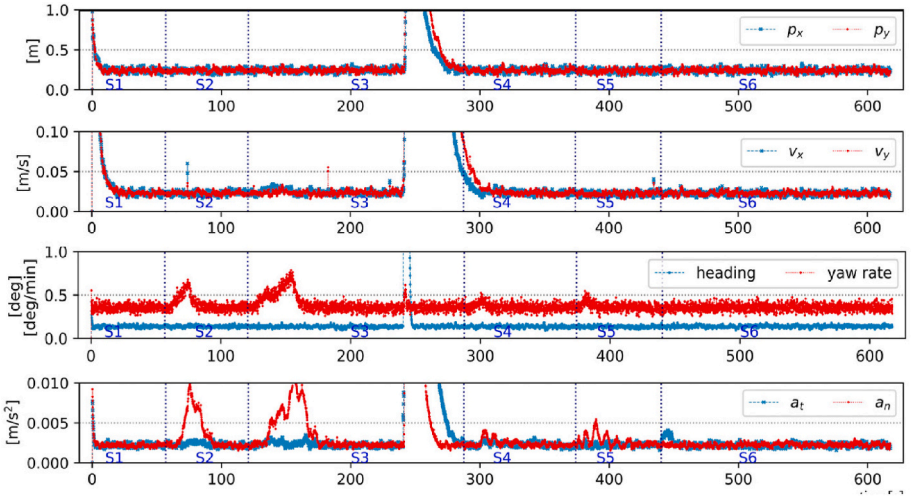

Fig. 11. The RMS errors of estimated states (50 runs) in Scenario 2 (CMM + UKF).

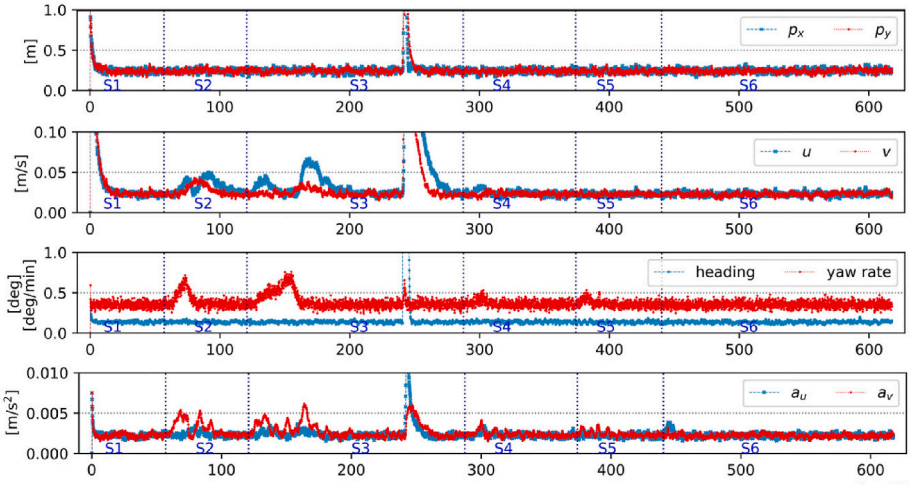

Fig. 12. The RMS errors of estimated states (50 runs) in Scenario 3 (CTRA + EKF).

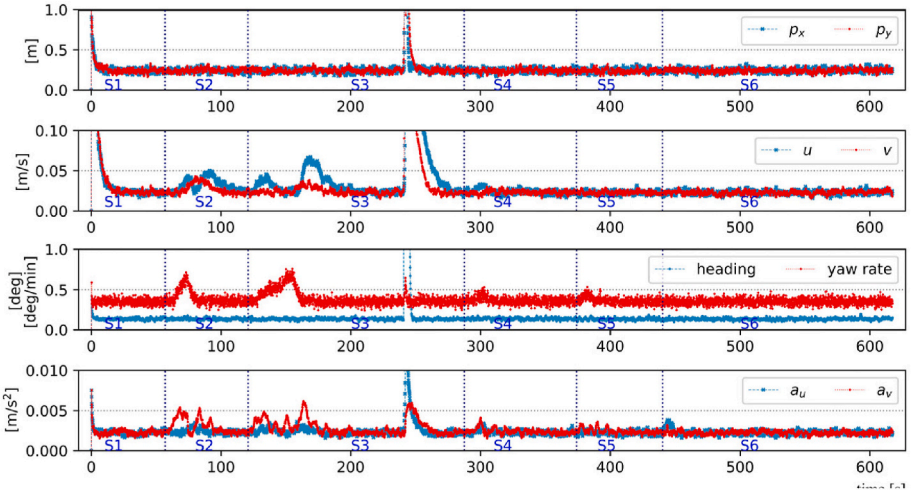

Fig. 13. The RMS errors of estimated states (50 runs) in Scenario 4 (CTRA + UKF).

CRediT authorship contribution statement

Yufei Wang: Conceptualization, Methodology, Programming, Validation, Writing – original draft, preparation. **Lokukaluge Prasad Perera:** Methodology, Validation, Supervision, Writing – review & editing. **Bjørn-Morten Batalden:** Supervision, Writing – review & editing.

Declaration of competing interest

The authors declare that they have no known competing financial interests or personal relationships that could have appeared to influence the work reported in this paper.

Data availability

Data will be made available on request.

References

Akbar, A., Aasen, A., Msakni, M.K., Fagerholt, K., Lindstad, E., Meisel, F., 2020. An economic analysis of introducing autonomous ships in a short-sea liner shipping network. Int. Trans. Oper. Res. 28 https://doi.org/10.1111/itor.12788.

Ames, William F., 1977. Numerical Methods for Partial Differential Equations, second ed. Academic Press, pp. 1–40. 9780120567607.

Barrau, A., 2015. Non-linear state error based extended Kalman filters with applications to navigation. Automatic. Mines Paristech, English. NNT:. tel-01247723.

Bar-Shalom, Y., Rong, X., L, Kirubarajan, T., 2002. Estimation with applications to tracking and navigation: theory. Algorithms and Software.John Wiley & Sons, Inc. 5, 247.

Best, R.A., Norton, J.P., 1997. A new model and efficient tracker for a target with curvilinear motion. IEEE Trans. Aero. Electron. Syst. 33, 1030–1037.

Butcher, J., 1996. A history of Runge-Kutta methods. Appl. Numer. Math. 20, 247–260. https://doi.org/10.1016/0168-9274(95)00108-5. URL: https://www.sciencedirect.com/science/article/pii/0168927495001085.

Chakraborty, D., Başağaoğlu, H., Winterle, J., 2020. Interpretable vs. noninterpretable machine learning models for data-driven hydro- climatological process modeling. Expert Syst. Appl. 170, 114498 https://doi.org/10.1016/j.eswa.2020.114498.

Chew, V., 1966. Confidence, prediction, and tolerance regions for the multivariate normal distribution. J. Am. Stat. Assoc. 61, 605–617. URL: http://www.jstor.org/stable/2282774.

Cline, A.K., Moler, C.B., Stewart, G.W., Wilkinson, J.H., 1979. An estimate for the condition number of a matrix. SIAM J. Numer. Anal. 16, 368–375. https://doi.org/10.1137/0716029.

Coraddu, A., Oneto, L., Baldi, F., Cipollini, F., Atlar, M., Savio, S., 2019. Data-driven ship digital twin for estimating the speed loss caused by the marine fouling. Ocean Engineering 186, 106063. https://doi.org/10.1016/j.oceaneng.2019.05.045.

Daum, F., 2005. Nonlinear filters: beyond the kalman filter. IEEE Aero. Electron. Syst. Mag. 20, 57–69. https://doi.org/10.1109/MAES, 2005.1499276.

Do, K.D., Pan, J., 2009. Control of Ships and Underwater Vehicles, 1 ed. Springer London. https://doi.org/10.1007/978-1-84882-730-1.

EMSA, 2021. Annual Overview of Marine Casualties and Incidents 2021. European Maritime Safety Agency. Report.

Endsley, M.R., 1995. Toward a theory of situation awareness in dynamic systems. Hum. Factors 37, 32–64. https://doi.org/10.1518/001872095779049543.

Fossen, T.I., 2010. Handbook of Marine Craft Hydrodynamics and Motion Control. John Wiley & Sons Ltd.

Frogerais, P., Bellanger, J., Senhadji, L., 2012. Various ways to compute the continuous-discrete extended kalman filter. IEEE Trans. Automat. Control 57, 1000–1004.
Grech, M.R., Horberry, T., Smith, A., 2002. Human error in maritime operations: analyses of accident reports using the leximancer tool. In: Proceedings of the Human Factors and Ergonomics Society Annual Meeting, vol. 46, pp. 1718–1721. https://doi.org/10.1177/154193120204601906.
Hanachi, H., Yu, W., Kim, I.Y., Liu, J., Mechefske, C., 2019. Hybrid data-driven physics-based model fusion framework for tool wear prediction. Int. J. Adv. Des. Manuf. Technol. 101 https://doi.org/10.1007/s00170-018-3157-5.
Hover, F.S., Michael S, T., 2010. Chapter 10: vehicle internal dynamics. In: System Design for Uncertainty. MIT OpenCourseWare, Cambridge MA. URL: https://ocw.mit.edu/courses/2-017j-design-of-electromechanical-robotic-systems-fall-2009/resources/mit2_017jf09_ch10/.MIT.
Ian, C., 2004. Ship Dynamics for Mariners. The Nautical Institute, p. 114.
Im, I., Shin, D., Jeong, J., 2018. Components for smart autonomous ship architecture based on intelligent information technology. Proc. Comput. Sci. 134, 91–98. https://doi.org/10.1016/j.procs.2018.07.148.
Janssen, W.D., Blocken, B., van Wijhe, H.J., 2017. Cfd simulations of wind loads on a container ship: Validation and impact of geometrical simplifications. J. Wind Eng. Ind. Aerod. 166, 106–116. URL: https://www.sciencedirect.com/science/article/pii/S0167610517300818.
Kim, T.E., Perera, L.P., Sollid, M.P., Batalden, B.M., Sydnes, A., 2022. Safety challenges related to autonomous ships in mixed navigational environments. WMU J. Marit.Aff. https://doi.org/10.1007/s13437-022-00277-z.
Kongsberg, M., 2020. Kongsberg maritime and massterly to equip and operate two zero-emission autonomous vessels for asko. URL:https://www.kongsberg.com/maritime/about-us/news-and-media. . (Accessed 20 September 2022).
Kretschmann, L., Burmeister, H.C., Jahn, C., 2017. Analyzing the economic benefit of unmanned autonomous ships: an exploratory cost- comparison between an autonomous and a conventional bulk carrier. Res. Transport. Bus. & Manag. 25, 76–86. URL: https://www.sciencedirect.com/science/article/pii/S2210539516301328.
Leander, J., Lundh, T., Jirstrand, M., 2014. Stochastic differential equations as a tool to regularize the parameter estimation problem for continuous time dynamical systems given discrete time measurements. Math. Biosci. 251, 54–62. https://doi.org/10.1016/j.mbs.2014.03.001. URL: https://www.sciencedirect.com/science/article/pii/S0025556414000510.
Li, X.R., Jilkov, V.P., 2003. Survey of maneuvering target tracking. part i. dynamic models. IEEE Trans. Aero. Electron. Syst. 39, 1333–1364.
Mbalawata, I., Särkkä, S., Haario, H., 2012. Parameter estimation in stochastic differential equations with Markov chain Monte Carlo and non- linear kalman filtering. Comput. Stat. 28 https://doi.org/10.1007/s00180-012-0352-y.
Meguri2040, 2020. The nippon foundation meguri2040 fully autonomous ship program. URL: https://www.nippon-foundation.or.jp/en/news/articles/2022/20220118-66716.html. (Accessed 20 September 2022).
Miguel, M.R., Felipe, E., Alfredo, G., 2017. Analysis of the optimal sampling rate for state estimation in sensor networks with delays. ISA (Instrum. Soc. Am.) Trans. 68, 293–301. https://doi.org/10.1016/j.isatra.2017.03.007.
Molland, A., 2008. The Maritime Engineering Reference Book, 1 ed. Butterworth-Heinemann.
MSC, 2021. Outcome of the Regulatory Scoping Exercise for the Use of Maritime Autonomous Surface Ships (MASS).Report MSC.1/Circ.1638. Maritime Safety Committee IMO.
Munim, Z.H., 2019. Autonomous ships: a review, innovative applications and future maritime business models. Supply Chain Forum Int. J. 20, 266–279. https://doi.org/10.1080/16258312.2019.1631714.
Murray, B., Perera, L.P., 2020. A dual linear autoencoder approach for vessel trajectory prediction using historical ais data. Ocean Engineering 209, 107478. https://doi.org/10.1016/j.oceaneng.2020.107478.
Perera, L.P., 2017. Navigation vector based ship maneuvering prediction. Ocean Engineering 138, 151–160.
Perera, L.P., 2019. Deep learning toward autonomous ship navigation and possible colregs failures. J. Offshore Mech. Arctic Eng. 142 https://doi.org/10.1115/1.4045372.
Perera, L.P., Murray, B., 2019. Situation awareness of autonomous ship navigation in a mixed environment under advanced ship predictor. In: ASME 2019 38th International Conference on Ocean. Offshore and Arctic Engineering. V07BT06A029.
Rahman, S.M., San, O., Rasheed, A., 2018. A hybrid approach for model order reduction of barotropic quasi-geostrophic turbulence. Fluid 3, 86. https://doi.org/10.3390/fluids3040086.
Ribeiro, M.T., Singh, S., Guestrin, C., 2016. Model-agnostic interpretability of machine learning. URL: https://arxiv.org/abs/1606.05386.
Sandhåland, H., Oltedal, H., Eid, J., 2015. Situation awareness in bridge operations – a study of collisions between attendant vessels and offshore facilities in the north sea. Saf. Sci. 79, 277–285. https://doi.org/10.1016/j.ssci.2015.06.021.
Sarkka, S., 2007. On unscented kalman filtering for state estimation of continuous-time nonlinear systems. IEEE Trans. Automat. Control 52, 1631–1641.
Schubert, R., Richter, E., Wanielik, G., 2008. Comparison and Evaluation of Advanced Motion Models for Vehicle Tracking, pp. 1–6. https://doi.org/10.1109/ICIF.2008.4632283.
Seo, S., 2016. Safer and more efficient ship handling with the pivot point concept. The Int.J.Marine Navig.Safety of Sea Transport. 10.
Sneddon, A., Mearns, K., Flin, R., 2006. Situation awareness and safety in offshore drill crews. Cognit. Technol. Work 8, 255–267. https://doi.org/10.1007/s10111-006-0040-1.
Stellet, J.E., Straub, F., Schumacher, J., Branz, W., Zöllner, J.M., 2015. Estimating the process noise variance for vehicle motion models. In: 2015 IEEE 18th International Conference on Intelligent Transportation Systems, pp. 1512–1519. https://doi.org/10.1109/ITSC.2015.212.
Svensson, D., 2019. Derivation of the discrete-time constant turn rate and acceleration motion model. In: 2019 Sensor Data Fusion: Trends, Solutions, Applications. SDF), pp. 1–5. https://doi.org/10.1109/SDF.2019.8916654.
Takeno, M., Katayama, T., 2012. A numerical method for continuous-discrete unscented kalman filter. Int. J. Innovat. Comput. Inf. Control 8-3 (B), 2261–2274.
Thombre, S., Zhao, Z., Ramm-Schmidt, H., Vallet García, J.M., Malkamäki, T., Nikolskiy, S., Hammarberg, T., Nuortie, H., Bhuiyan, H., M, Z., Särkkä, S., Lehtola, V. V., 2022. Sensors and ai techniques for situational awareness in autonomous ships: a review. IEEE Trans. Intelligent Transport. Sys. 23, 64–83. https://doi.org/10.1109/TITS.2020.3023957.
Triepels, R., Daniels, H., Feelders, A., 2018. Data-driven fraud detection in international shipping. Expert Syst. Appl. 99, 193–202. URL: https://www.sciencedirect.com/science/article/pii/S0957417418300083.
UNCTAD, 2021. Review of Maritime Transport 2021. Report. United Nations Conference on Trade and Development.
Vellido, A., Martín-Guerrero, J.D., Lisboa, P.J.G., 2012. Making machine learning models interpretable. In: European Symposium on Artificial Neural Networks, Computational Intelligence and Machine Learning.
Wan, E., Merwe, R., 2000. The Unscented Kalman Filter for Nonlinear Estimation, pp. 153–158. https://doi.org/10.1109/ASSPCC.2000.882463.
Wang, J., Li, Y., Gao, R.X., Zhang, F., 2022a. Hybrid physics-based and data-driven models for smart manufacturing: modelling, simulation, and explainability. J. Manuf. Syst. 63, 381–391. URL. https://www.sciencedirect.com/science/article/pii/S0278612522000541.
Wang, Y.F., Perera, L.P., Batalden, B.M., 2022b. The comparison of two kinematic motion models for shipping maneuvers (79583. In: The 42nd International Conference on Ocean, Offshore and Arctic Engineering (OMAE).
Wang, Y.F., Perera, L.P., Batalden, B.M., 2023. Coordinate conversion and switching correction to reduce vessel heading related errors in highlatitude navigation. In: The 22nd World Congress of the International Federation of Automatic Control. IFAC, 2023.
Willard, J.D., Jia, X., Xu, S., Steinbach, M.S., Kumar, V., 2020. Integrating Physics-Based Modeling with Machine Learning: A Survey, 04919. ArXiv abs/2003.
Wróbel, K., Montewka, J., Kujala, P., 2017. Towards the assessment of potential impact of unmanned vessels on maritime transportation safety. Reliab. Eng. Syst. Saf. 165, 155–169. URL: https://www.sciencedirect.com/science/article/pii/S0951832016303337.
Yara, I., 2021. Yara to start operating the world's first fully emission-free container ship. URL. https://www.yara.com/corporate-releases/yara-to-start-operating-the-worlds-first-fully-emission-free-container-ship. (Accessed 20 September 2022).
Yasukawa, H., Yoshimura, Y., 2014. Introduction of mmg standard method for ship maneuvering predictions. J. Mar. Sci. Technol. 20, 37–52. https://doi.org/10.1007/s00773-014-0293-y.